Journal of Molecular Liquids 332 (2021) 115864

Contents lists available at ScienceDirect

Journal of Molecular Liquids

journal homepage: www.elsevier.com/locate/molliq

Insights on biodiesel blends with alkanol solvents

H. Ghazipour [a], A. Gutiérrez [b], D. Mohammad-Aghaie [a], M.M. Alavianmher [a], S.M. Hosseini [c,*], S. Aparicio [b,*]

[a] Department of Chemistry, Shiraz University of Technology, Shiraz 71555-313, Iran
[b] Department of Chemistry, University of Burgos, 09001 Burgos, Spain
[c] Department of Chemistry, University of Hormozgan, Bandar Abbas 71961, Iran

ARTICLE INFO

Article history:
Received 24 July 2020
Received in revised form 29 January 2021
Accepted 4 March 2021
Available online 8 March 2021

Keywords:
Biodiesel
Fatty acid esters
Alkanol
Thermophysics
Hydrogen bonding
Molecular modelling

ABSTRACT

Thermophysical properties of mixtures of fatty acid esters with alkanols were measured in the whole composition range as a function of temperature for understanding features of biodiesel blends. Excess and mixing properties calculated from experimental measurements allowed to quantify and analyze the intermolecular forces in the considered systems. Likewise, molecular modelling studies using quantum chemistry and classical molecular dynamics simulations led to a detailed characterization of these systems at the nanoscopic level. The nature of hydrogen bonding in these liquid mixtures was particularly analyzed from macroscopic properties and theoretical modelling results. The reported experimental and computational study allowed to infer the relationships between the intermolecular forces and additional microscopic features and the mixtures macroscopic properties, which are relevant for the development and characterization of biodiesels. The non-ideality behavior of the studied systems shows relevant changes in hydrogen bonding structuring upon mixing, with the fatty acid esters largely disrupting the alcohols self-association, although ester – alcohol hydrogen bonding is developed, this type of interactions is remarkably weaker than those for alcohols. Therefore, the studied biodiesel blends macroscopic properties may be tuned and controlled through the amount of alcohols in the mixtures and rooted on its effect on hydrogen bonding.

1. Introduction

Biofuels, such as biodiesels [1], have been proposed as renewable alternatives to fossil fuels to minimize greenhouse gas emissions [2], general pollutants reduction [3] as well as reducing the dependence on non-renewable energy sources [4] with suitable economics [5]. Biodiesel is chemically composed of mono alkyl (methyl/ethyl) esters of long chain fatty acids (FAE) [6], which can be derived from a large collection of different feedstocks [7] such as renewable vegetable oils, animal fats or their mixtures [8]. Biodiesels are mostly produced by the trans-esterification catalyzed reaction of vegetable oils or animal fats with monohydric alcohols, mainly methanol or ethanol, resulting in FAEs with methyl or ethyl groups [9,10]. The type of FAEs, i.e. degree of saturation and chain lengths, relies on the considered oil feedstocks [8,10] and determines the quality and stability of the final produced biodiesel [11] as well as the biodiesel engine performance and the developed emissions [12]. Therefore, biodiesels have large advantage over diesels derived from non-renewable fossil sources for compression internal combustion engines [13]. The performance of diesel engines using biodiesels as fuel has been studied considering different types of fuels and engines adjustments, with a decrease in the toxic gas emissions (such as CO or NOx) without affecting combustion engine efficiency. Nevertheless, other effects such as shorter ignition delay or higher break specific fuel consumption for biodiesel require adaptation of the engines for using biodiesels [14,15]. Likewise, relevant thermophysical properties of neat biodiesels, such as their higher density or viscosity in comparison with regular diesel have large effects on the injection and combustion processes, and thus, on the engine's performance [16]. The thermophysical properties of biodiesels can be improved [17] and fine-tuned by using alcohols as additives [18], thus allowing suitable engines performance [19]. Alcohols such as 2-butanol (2BUT), 2-methyl-1-butanol (2M1BUT) or 1-2-butanediol (12BD) have been proposed to improve biodiesels

Abbreviations: FAE, long chain fatty acids; 2BUT, 2-butanol; 2M1BUT, 2-methyl-1-butanol; 12BD, 1-2-butanediol; MC, methyl caprate; EM, ethyl myristate; DFT, density functional theory; MD, molecular dynamics; AIM, Atoms in a Molecule; RDG, Reduced density Gradient; BSSE, Basis Set Superposition Error; BCP, binary critical point from DFT – AIM; HOMO, high occupied molecular orbital; LUMO, low unoccupied molecular orbital; RDF, radial distribution function; SDF, Spatial Distribution Functions; ρ, density; u, speed of sound; γ, surface tension; n_D, refraction index; D, self-diffusion coefficient; V_m^E, excess molar volume; Δu, change in the speed of sound; Δk_S, change in the isentropic compressibility; α_p^E, excess thermal expansion coefficient; V_i^*, molar volume of pure i compound; $\overline{V}_i$, partial molar volume of compound i; $\overline{V}_i^\infty$, partial molar volumes at infinite dilution of compound i; $\overline{V}_i^{E,\infty}$, excess partial molar volumes at infinite dilution of compound i; E_{inter}, intermolecular interaction energy from molecular dynamics simulations; N_H, average number of hydrogen bonds from molecular dynamics simulations.

* Corresponding authors.
E-mail addresses: sm.hosseini@hormozgan.ac.ir (S.M. Hosseini), sapar@ubu.es (S. Aparicio).

https://doi.org/10.1016/j.molliq.2021.115864
0167-7322/

performance [20]. Hence, the knowledge of biodiesel + alcohol mixtures thermophysical properties is required for the analysis of their suitability for internal combustion engines.

The fatty acid profile of biodiesel corresponds to that of its feedstock [21] and it has a major role on the properties of the developed biodiesel [22]. FAEs derived from medium size saturated acids, like capric (C_{10}) and myristic ones (C_{14}), are present in vegetable oils [23], like coconut one, which have been proposed for biodiesel production and allow the obtention of kerosene or jet fuels [24]. The fatty acid composition of oils is largely dependent on the source and it has a large effect on the emissions and engines performance [25], with different content in saturated and unsaturated esters as well as considering the alkyl chain lengths. In the case of coconut oils, 91.9% is composed of saturated fatty acids, with 89% of these saturated acids having lower than 14 carbon atoms. Therefore, these coconut oils are mainly composed of saturated short chain (<14) acids [23]. Although in other vegetable oils, unsaturated and longer fatty acids prevail (such as oleic or linoleic acids) [26], to study short and saturated fatty acids is representative of certain types of vegetable oils (such as coconut ones) and to consider the light fraction of other oils. Therefore, this paper reports a theoretical and experimental study on the properties of methyl caprate (MC) and ethyl myristate (EM), as model FAEs from vegetable (coconut) oil feedstocks and their light fractions, as well as their blends, with 2BUT, 12BD and 2M1BUT alcohols, Fig. 1, over the whole composition range and as a function of temperature. The thermophysical characterization reported in this work provides the required information to characterize biodiesel + alcohol blends performance to be suitably used in combustion engines [27,28]. Likewise, the design of suitable biodiesels and blends [29] requires understanding the relationships between the biodiesel chemical composition, intermolecular forces and macroscopic physicochemical properties, which affect their performance. Literature studies have proved the suitability of molecular modelling, e.g. molecular dynamics (MD) simulations, to characterize the properties and structuring of biodiesel blends, with attention to intermolecular forces and nanoscopic structuring [30,31], or for the study of relevant physicochemical properties like tribological ones [32]. Likewise, MD studies have probed to infer the molecular level roots of physicochemical properties and fuels' miscibility in blends. For biodiesel as additive to diesel – ethanol fuels, de Oliveira et al. [33] probed the interaction of ethanol with the diesel and the FAEs though hydrogen bonding, thus acting as a miscibilization agent providing the ethanol dispersion into diesel. Thus, a theoretical study using quantum chemistry and molecular dynamics simulations was developed in this work for the same systems FAE + alcohol blends considered in the experimental research allowing a detailed characterization at the nanoscopic level. In this way, the combined experimental and theoretical study on the considered model biodiesel blends would allow to develop structure-property relationships [34,35], which may allow the design of more suitable biodiesel formulations as alternative to non-renewable diesels.

2. Materials and methods

2.1. Chemicals

The sources and purities of chemical used in this work for the experimental study are reported in Table S1 (Supplementary Information). In order to verify the purity of the pure chemicals, thermophysical properties were measured and compared with the literature values, as shown in Tables S2 and S3 (Supplementary Information) showing satisfactory agreements.

2.2. Apparatus and procedures

All FAEs + alcohol blends were freshly prepared before each experiment by weighing suitable amounts on an analytical balance (Sartorius TE124S, ± 1 10^{-5} g), and stored in airtight flasks. Samples were degassed (20 min) by means of an ultrasound device (MISONIX Ultrasonic Liquid Processors).

Density, ρ, and speed sound, u, were simultaneously measured with an Anton Paar DSA 5000 vibrating tube densitometer and sound analyzer, with the certified precisions of $\pm 1 \times 10^{-6}$ g cm^{-3} and ± 0.01 m s^{-1}, respectively. Peltier elements together with two integrated Pt100 thermometers, controlled and measured the cells temperature (±1 10^{-3} K). The DSA 5000 automatically corrects the viscosity-related errors, by measuring the damping effect of

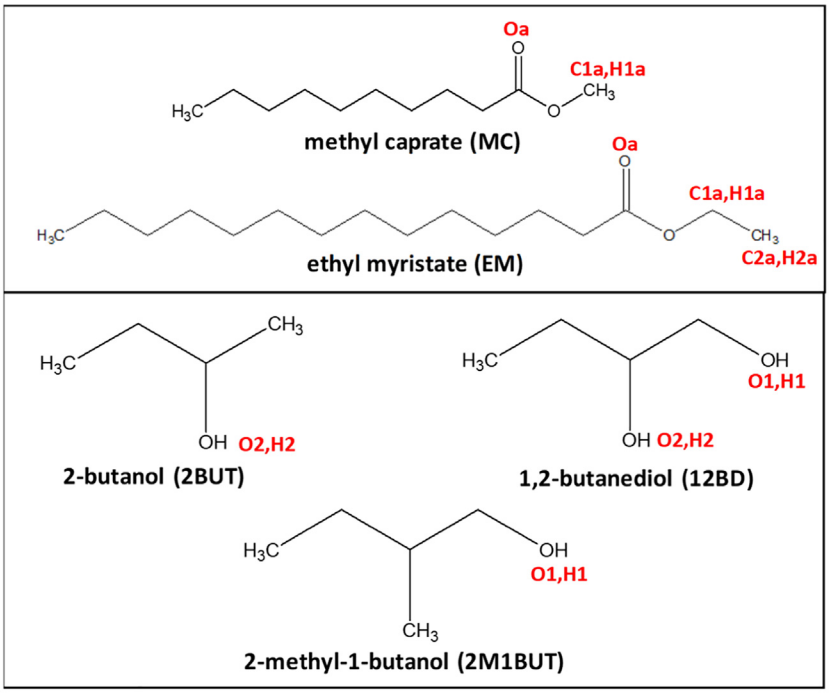

Fig. 1. Molecules considered in this work.

the sample. Calibrations with dry air and deionized water were carried out.

Refraction index, n_D, was measured with regard to sodium D-line using an Anton Paar Abbemat 200 refractometer, with ±0.0001 specified accuracy. The cell temperature is controlled with a built-in high-end peltier unit, ± 0.05 K.

Surface tension, γ, was measured with a capillary apparatus, Fig. S1 (Supplementary Information). The capillary apparatus was sealed under vacuum to assure the surface tension measurement at liquid/vapor interface in equilibrium and under vapor saturation pressure. In order to calibrate the inner size of the standard capillary, it was partially filled with mercury of the known density of 13.53359 g cm^{-3} at 298.15 K. This density value along with the net weight of mercury and its column length (measured by micrometer within ±0.01 mm), were employed to determine the inner radius of the capillary. The calibration was repeated along the capillary (at different heights), in order to make sure about the uniformity of the capillary radius. In this study, a capillary with the inner radius of 0.52 mm was used for all measurements. After loading the capillary apparatus with solution, the system was cooled in the ice bath for one hour, while kept under vacuum (1.2 Pa). After elimination of dissolved atmospheric gases by complete evacuation, the capillary was sealed under vacuum, then transferred to an oil bath thermostat for the surface tension measurement. The temperature was controlled by an oil bath thermostat, ± 0.5 K. A cathetometer comprising a digital camera was focused horizontally on the middle of the column of solution, raised in the capillary. The camera was interfaced with a personal computer in order to determine the absolute solution height, within ±0.005 mm.

After the measurements of mentioned thermodynamics properties, expanded uncertainties in refractive indices, densities, speeds of sound and surface tensions, were found to be ±0.0003 n_D, ± 0.00003 g cm^{-3}, ± 0.05 m s^{-1} and ± 0.3 mN m^{-1}, respectively.

2.3. Molecular modelling

The ORCA program [36] was used for DFT calculations along this work. Dimers of 1 {MC or EM} + 1 {2BUT or 2M1BUT or 12BD} were built and energy optimizations were carried out at B3LYP [37,38,39] plus 6–311++G** theoretical level, with van der Waals interactions treated with Grimme's method (DFT-D3) [40]. The intermolecular forces were topologically analyzed according to Atoms in a Molecule (AIM [41]) and Reduced density Gradient (RDG, [42]) methods in the MultiWFN software [43]. The interaction energy, E_{int}, for each considered dimer was calculated as the energy difference of the dimer and the sum of the energies of the corresponding monomers, all calculated at the same theory level, with Basis Set Superposition Error (BSSE) corrected using counterpoise method [44]. Atomic charges for the optimized structures of the dimmers were calculated using the ChelpG method [45].

Classical MD simulations to model the liquid mixtures behaviour were carried out using MDynaMix v.5.2 [46] program. Simulations for {MC or EM} + {2BUT or 2M1BUT or 12BD} systems were carried in the full composition range. Initial cubic simulation boxes (with box size in the 46 to 61 Å range, depending on the molecules and mixture composition) containing 500 total molecules were built using Packmol [47] program, with the fatty acid ester and alkanol number of molecules being varied according to each particular considered mole fraction. The force field parameterizations used along this work are reported in Table S4 (Supplementary Information). Force field parameters were obtained from SwissParam database, Merck Molecular Force Field [48], except atomic charges which were inferred from ChelpG charges obtained from DFT simulations of isolated monomers. MD simulations for all the considered systems were carried out in a two steps procedure: *i*) 10 ns long simulations in the NVT ensemble at 313 K for equilibration purposes, assured by constancy of total potential energy, then followed by *ii*) 50 ns long simulations in the NPT ensemble at 313 K and 1 bar for production runs. The moderate viscosity of the studied systems, with the larger viscosity being for pure 12BD at 313.15 K (21.49 mPa s [49]) assures suitable simulation time for obtaining reliable results. Nevertheless, fully diffusive regime was assured for all the simulations by analysing log-log plots of mean square displacements vs simulation time leading to slopes in the 0.98 to 1.00 range for all the considered pure compounds and blends. All MD simulations were carried out using Tuckerman–Berne double time step algorithm [50] for solving the equations of motion, 1 and 0.1 fs for long and short time steps. Several tests were run for the selection of long timestep, with the results probing more stable dynamics for 1 fs than for larger times. Ewald method [51] (15 Å for cut-off radius) was applied for handling electrostatic interactions. Lennard-Jones interactions were treated with 15 Å cut-off distance and Lorentz-Berthelot mixing rules for cross terms. Temperature and pressure were controlled with Nose-Hoover method.

3. Results and discussion

3.1. Experimental study

Experimental values of density and speed of sound for FAEs + alcohol blends in the whole composition range and in the 293.15 to 333.15 K

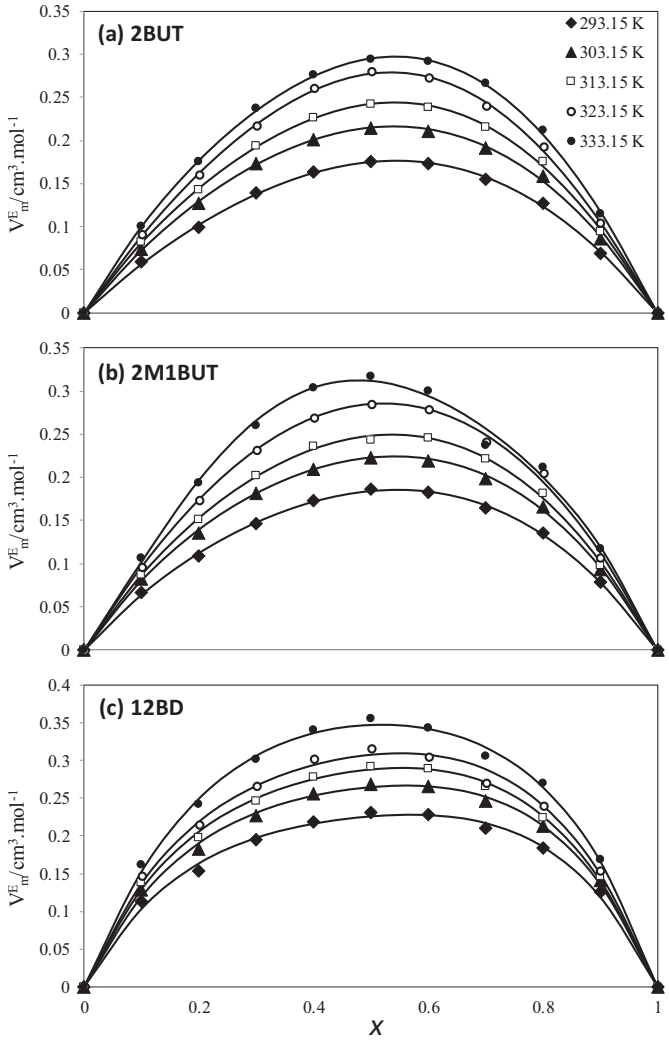

Fig. 2. Excess molar volumes, V_m^E, of *x* MC + (1-*x*) {2BUT, 2M1BUT or 12BD} at different temperatures. Markers represent the calculated excess molar volumes using the Eq. 1, while solid lines are the result of fitting these data with the Redlich-Kister polynomial equation, Eq. 8 (Supplementary information).

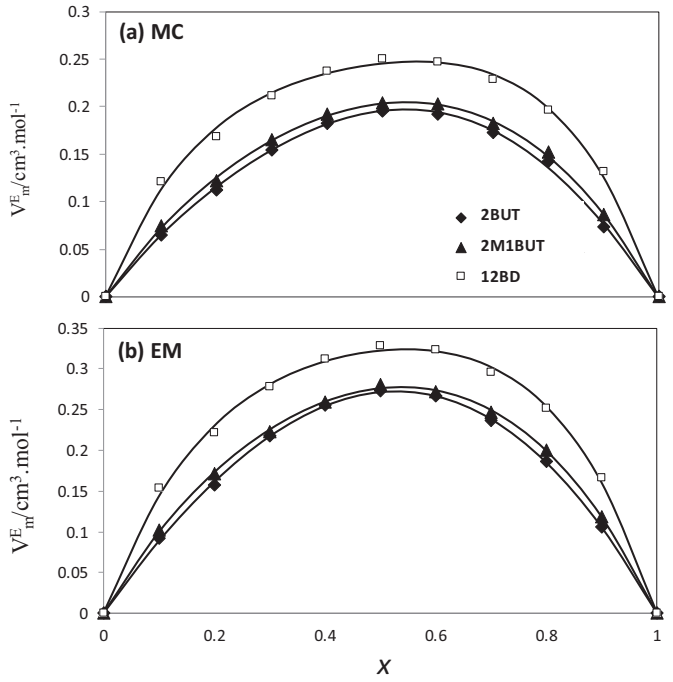

Fig. 3. Excess molar volumes, V^E_m, of x {MC or EM} + (1-x) {2BUT, 2M1BUT or 12BD} at T = 298.15 K. Markers represent the calculated excess molar volumes using the Eq. 1, while solid lines are the result of fitting these data with the Redlich-Kister polynomial equation, Eq. 8 (Supplementary information).

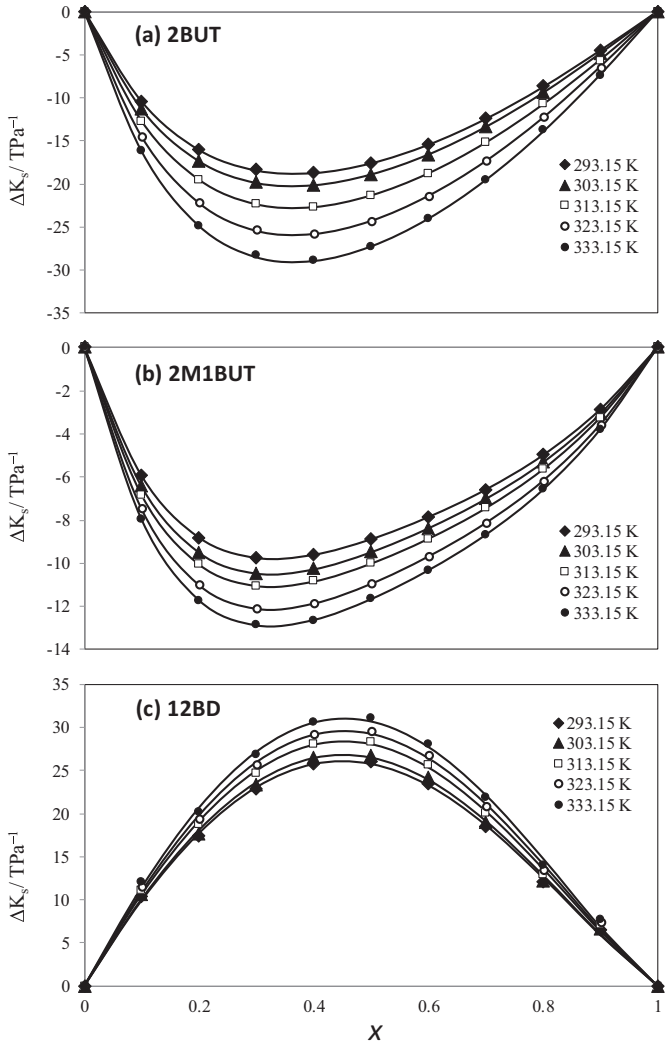

Fig. 4. Change in isentropic compressibility, Δk_S, of x EM + (1-x) {2BUT, 2M1BUT or 12BD} at different temperatures. Markers represent the calculated change in isentropic compressibilities using the Eq. 3, while solid lines are the result of fitting these data with the Redlich-kister polynomial equation, Eq. 8 (Supplementary information).

temperature range are reported in Tables S5 to S10 (Supplementary Information). From these properties, excess molar volume, V^E_m, change in the speed of sound, Δu, change in the isentropic compressibility, Δk_S, and excess thermal expansion coefficient, α^E_P, were calculated according to the thermodynamic expressions reported in the Supplementary Information. The V^E_m, Δu, Δk_S, α^E_P, evolution vs blends composition (defined with FAEs mole fraction, x) were fitted to Redlich-Kister functions, with the fitting coefficients being reported in Tables S11 and S12 (Supplementary Information). Likewise, partial molar volumes at infinite dilution for each compound in the blends, $\overline{V}_i^{\infty}$ and the corresponding excess values at infinite dilution, $\overline{V}_i^{E,\infty}$, were calculated and reported in Tables S13 and S14 (Supplementary Information). Experimental values for n_D and γ in the blends are reported in Tables S15 and S16 (Supplementary information).

The values of V^E_m for all studied mixtures are positive in the 293.15 to 333.15 K temperature range, Tables S5 to S10 (Supplementary Information) and Figs. 2 and 3, thus indicating expansion upon mixing and thus weaker attractive interactions between the unlike molecules than the like ones. It is noteworthy that the V^E_m mainly depends on the variation of intermolecular forces and the molecular packing resulting from difference in the size and shape of mixture components. The alcohols studied in this work can self-associate forming strong hydrogen bonds. On the other hand, MC and EM FAEs are polar molecules, and thus, the considered FAEs are self-associated by dipole – dipole interaction. In MC/EM – alcohol blends, the hydroxyl group(s) in the alcohols may develop heteroassociations with the FAEs by hydrogen bonding with oxygen atom of carbonyl group. Nevertheless, the positive V^E_m confirms that the disruption of alcohol-alcohol self-association prevails over the newly developed alcohol – FAEs heteroassociation by hydrogen bonding, i.e. the disruptive effect of FAEs is not compensated by the development of weaker FAE – alcohol hydrogen bonds. The disruptive effect of FAEs is confirmed in Fig. 3, which shows larger V^E_m for a fixed alcohol and V^E_m in the ordering 12BD > 2M1BUT ~ 2BUT. Therefore, the presence of a larger alkyl chain in EM (C_{14}) in comparison with MC (C_{10}) induces larger disruption on alcohols self-hydrogen bonding network. Likewise, the presence of two hydroxyl groups in 12BD, i.e. a larger hydrogen bonding network, leads to larger changes upon mixing with FAEs, i.e. larger V^E_m. The temperature effect on V^E_m as reported in Fig. 2 shows more positive V^E_m with increasing temperature for all binary systems, over the whole composition range. Temperature increase leads to break the weak dipole-dipole interactions of the FAEs and even the hydrogen bonding network of alcoholic solvents, leading into the more positive V^E_m. As observed in Figs. 2 and 3, the maximum value of V^E_m occurs at about equimolar composition, for all the studied binary mixtures. Therefore, the sign, values and composition changes of V^E_m indicate that like interactions (hydrogen bonds between the alcohol molecules and dipole-dipole interactions in methyl/ethyl ester molecules) are going to break upon mixing, being not balanced by the unlike weaker interactions which are forming.

The remaining thermophysical properties determined in this work provide additional clues on the behavior of the studied blends. Values for Δk_s (Fig. 4) are negative for 2BUT and 2M1BUT containing mixtures, whereas those with 12BD are positive in the whole composition range. These results confirm the role of alcohol self-association by hydrogen bonding and its disruption upon mixing with FAEs on the studied blends properties, the larger extension of hydrogen bonding in 12BD mixtures

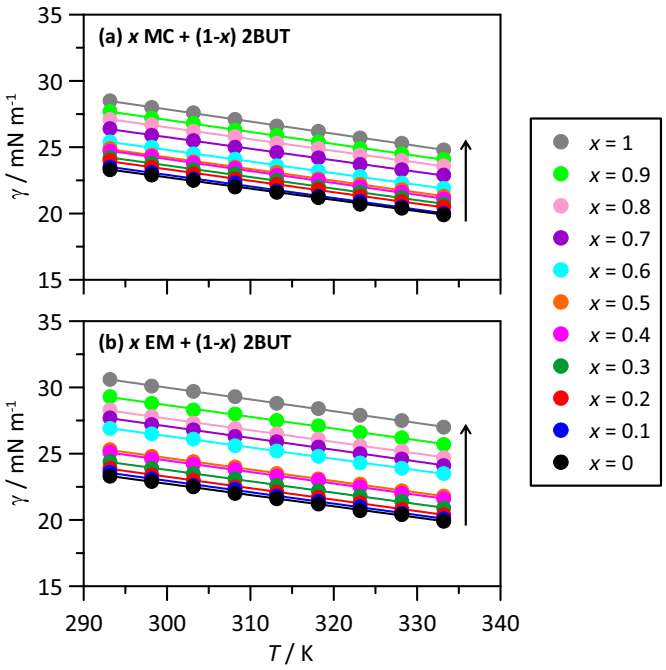

Fig. 5. Surface tension, γ, for (a) x MC + (1-x) 2BUT and (b) x EM + (1-x) 2BUT at different temperatures and mole fractions. Arrows indicate increasing FAE content.

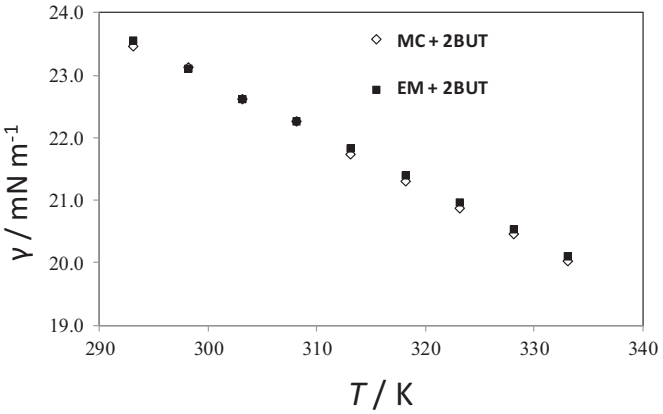

Fig. 6. Surface tension, γ, for x {MC or EM} + (1-x) 2BUT at different temperatures and x = 0.1.

leads to the positive Δk_s in contrast with the negative values for 2BUT and 2M1BUT. Therefore, 12BD mixtures are more compressible than neat 12BD because of disrupting effect by the FAEs presence, whereas the opposite effect is inferred for 2BUT and 2M1BUT. The increase of temperature leads to an increase in compressibility for the mixtures because of the weak FAE – alcohol interactions can be disrupted upon heating.

The values for Δu reported in Tables S5 to S10 (Supplementary Information) are negative for all the mixtures and temperatures corroborating the notion that the unlike interactions between mixture components are weaker than the like interactions between pure alcoholic solvents. It is noteworthy that the sign of Δu and its variation in all considered systems, are in complete accordance with the excess molar volume changes, supporting our explanations about the relationship between the intermolecular forces and V_m^E values. Numerical values of α_p^E for all binary mixtures are positive for all the cases, Tables S5 to S10 (Supporting Information), which indicate the rupture of hydrogen bonding between alcohol solvent molecules. Experimental n_D, Tables S13 and S14 (Supplementary Information), increases with the increase of MC and EM mole fractions for 2BUT and 2M1BUT, whereas the opposite effect is inferred for 12BD mixtures. This observation confirms the different nature of 12BD containing mixtures in terms of hydrogen bonding and it is consistent with the obtained results for the effect of intermolecular interactions on V_m^E, which in turn reveals the direct relationship between the refractive index and the effective intermolecular interactions.

Additional information on the developed interactions can be inferred from the partial molar volumes at infinite dilution, for which the infinitely diluted compound only develops heteoassociations which the prevailing solvent around it. Inspecting reported values in Tables S15 and S16 (Supplementary Information) reveals that pure molar volumes V_1^* and V_2^*, are smaller than the corresponding partial molar volumes at infinite dilution $\overline{V}_1^{\infty}$ and $\overline{V}_2^{\infty}$, for all studied binary mixtures. Positive $\overline{V}_1^{E,\infty}$ and $\overline{V}_2^{E,\infty}$ values indicate the volume expansion of these mixtures on mixing, which can be ascribed to the presence of significant interactions between like molecules.

Surface tension values for the studied binary mixtures have been reported in Tables S13 and S14 (Supplementary Information). Fig. 5 shows the plot of surface tension as a function of temperature for the MC + 2BUT blend at different mole fractions. Assessment of the data show that the surface tensions of all binary mixtures at the whole mole fraction range, decrease rather linearly with temperature. Surface tensions of MC + 2BUT and EM + 2BUT mixtures at the same mole fraction were compared in Fig. 6 indicating that both MC and EM have almost the same effect on the surface tension of 2BUT, as a solvent. Closer look at the obtained results shows that adding FAEs to pure 12BD leads to the decrease in surface tension value, while adding them to pure 2BUT increases this physical property. Again, this behavior which is consistent with our previous observations may be attributed to the nature and strength of like and unlike intermolecular interactions. The 12BD containing mixtures are largely affected by the presence of two hydroxyl groups in the alcohol, and thus having a larger hydrogen bonding network and so stronger intermolecular interactions, compared to 2BUT. Therefore, these two alcohols show different behavior toward mixing with the FAEs. Overall, it should be mentioned that interpretation of the surface tension data is generally not simple because in addition to the intermolecular interactions, the surface tension values are also affected by other factors, such as molecular orientation at surface.

3.2. Molecular modelling

The experimental study reported in the previous section provided clues on the nature and extension of intermolecular forces in the considered FAEs + alcohol blends. Although these macroscopic thermophysical properties are thus largely correlated with the underneath intermolecular interactions, which determine mixed fluids properties and structure, detailed nanoscopic information cannot be directly inferred from them. Therefore, molecular modelling studies, using both DFT and MD approaches, will provide the required nanoscopic characterization of the blends in terms of intermolecular interactions as well as additional features determining liquid structuring and properties.

The polarity of MC and EM molecules was probed by gas phase DFT calculations for isolated monomers leading to 1.6 (MC) and 1.7 (EM) D, respectively. DFT analysis were carried out for FAE + alcohol dimers, with the possible hydrogen bonding between the alcohol hydroxyl group and the carbonyl group being studied. The results in Fig. 7 show the development of MC / EM – alcohol interaction, for which the Hydrogen to Oxygen (1.9 Å) distance indicates that it may be classified as hydrogen bond. The strength of the FAE – alcohol interaction, quantified through E_{int}, indicates moderately strong forces (in the 0.30 to 0.35 eV) being slightly larger for EM than for MC and for 12BD than for the other alcohols, Table 1. The nature of the FAE – alcohol interaction is further analyzed using AIM method, a Binary Critical Point

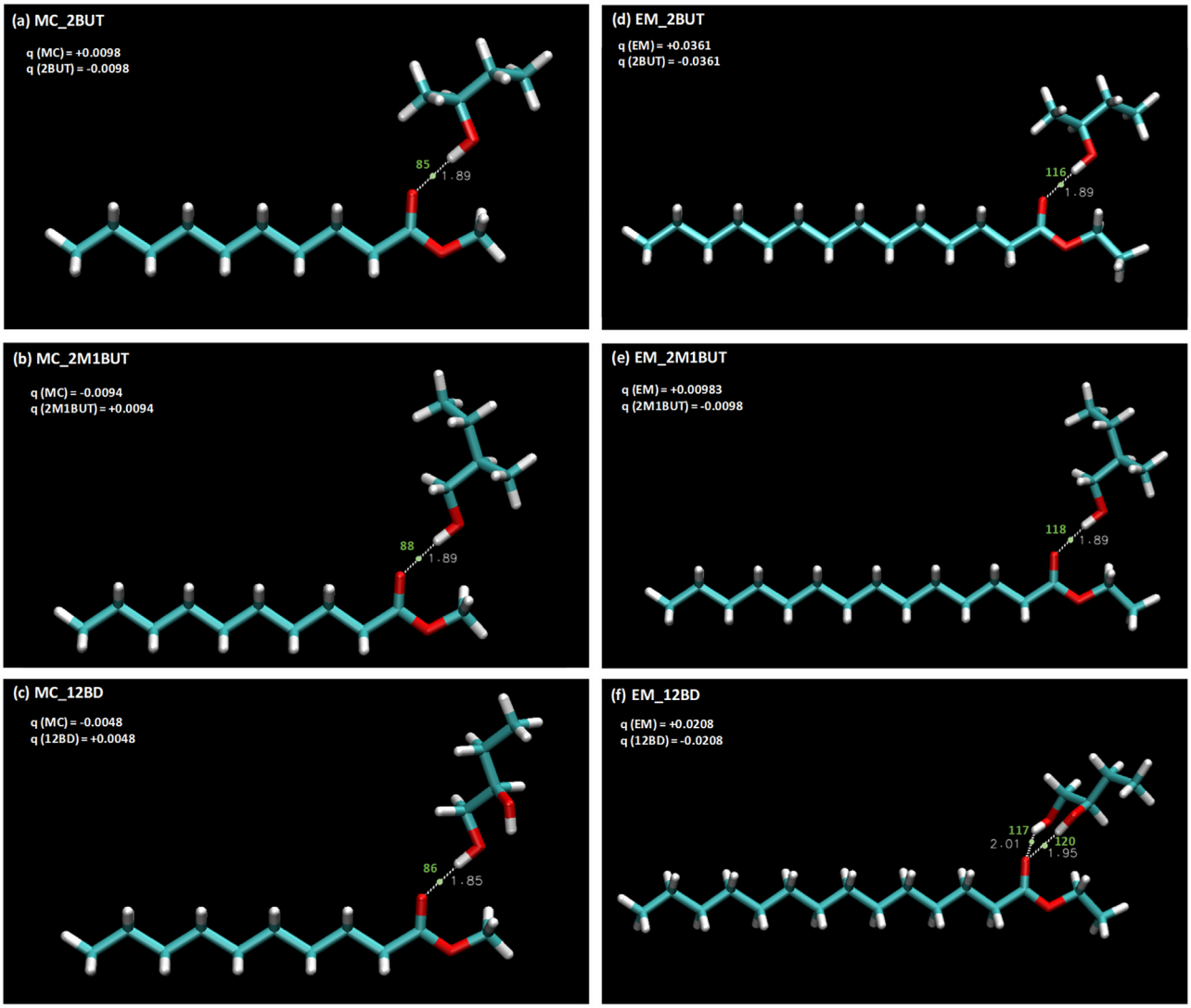

Fig. 7. Optimized structures for {MC or EM} + {2BUT, 2M1BUT or 12BD} dimmers calculated at B3LYP-D3/6–311++G** theory level. BCPs are indicated as green dots; dashed lines indicate relevant distances for hydrogen bonding with values in Å. Total ChelpG charges are indicated, *q*.

(type (3,-1) according to AIM naming, BCP) is developed in the bond path joining the donor and acceptor sites for the possible hydrogen bonding, Fig. 7. The properties of these BCPs are analyzed in Table 2 through the electron density, ρ, and its Laplacian, $\nabla^2\rho$. It has been proposed a scale for defining hydrogen bonding in terms ρ and $\nabla^2\rho$ at the BCPs placed between hydrogen bond donors and acceptors: *i*) 0.002 to 0.014 a.u. for ρ and *ii*) 0.014 to 0.139 a.u. for and $\nabla^2\rho$, with stronger interactions for larger values [52]. The ρ and $\nabla^2\rho$ values reported in Table 2 indicate moderately strong interactions, but they can be considered as hydrogen bonds according to the AIM criterion. Intermolecular interactions are also analysed using reduced density gradient (RDG) analysis, Figs. S2 and Fig. S3 (Supplementary Information). RDG analysis show the formation of blue spots along the line connecting hydrogen donor and acceptor, which correspond to moderately strong hydrogen bonding in agreement with AIM results. Likewise, green spots in the vicinity of the methylene ester group show van der Waals interactions through these sites, which also contributes to the strengthening of the FAE – alcohol intermolecular interactions. The development of

Table 1
Properties for fatty acid (MC or EM) + alkanols (2BUT, 2M1BUT or 12BD) dimmers calculated at B3LYP-D3/6–311++G** theory level. Counterpoise corrected interaction energy, (E_{int}); HOMO (E_{HOMO}) and LUMO (E_{LUMO}) energies; HOMO-LUMO energy gap (ΔE_G).

Structure	E_{int} / eV	E_{HOMO} / eV	E_{LUMO} / eV	ΔE_G / eV
MC + 2BUT	−0.314	−6.885	−0.337	−6.548
MC + 2M1BUT	−0.307	−6.891	−0.341	−6.550
MC + 12BD	−0.336	−7.047	−0.472	−6.575
EM + 2BUT	−0.326	−6.854	−0.340	−6.514
EM + 2M1BUT	−0.317	−6.873	−0.297	−6.576
EM + 12BD	−0.358	−6.883	−0.545	−6.338

Table 2
Atoms-in-a-molecule analysis of the reported fatty acid (MC or EM) + alkanols (2BUT, 2M1BUT or 12BD) dimmers calculated at B3LYP-D3/6–311++G** theory level. Bond critical points (BCP, (3, −1)) are provided in the table. Electron density (ρ) and Laplacian of electron density ($\nabla^2\rho$) at the corresponding BCP (labelling as in Fig. 7) are provided as a guide for AIM and RDG analysis.

Structure	BCP(s)	ρ / a.u.	∇^2ρ / a.u.	Interaction sites
MC + 2BUT	85	0.0263	0.1021	[MC](Oa)···(H4)[2BUT]
MC + 2M1BUT	88	0.0264	0.1026	[MC](Oa)···(H3)[2M1BUT]
MC + 12BD	86	0.0287	0.1107	[MC](Oa)···(H3)[12BD]
EM + 2BUT	116	0.0267	0.1033	[EM](Oa)···(H4)[2BUT]
EM + 2M1BUT	118	0.0265	0.1025	[EM](Oa)···(H3)[2M1BUT]
EM + 12BD	117	0.0204	0.0793	[EM](Oa)···(H3)[12BD]
	120	0.0234	0.0896	[EM](Oa)···(H4)[12BD]

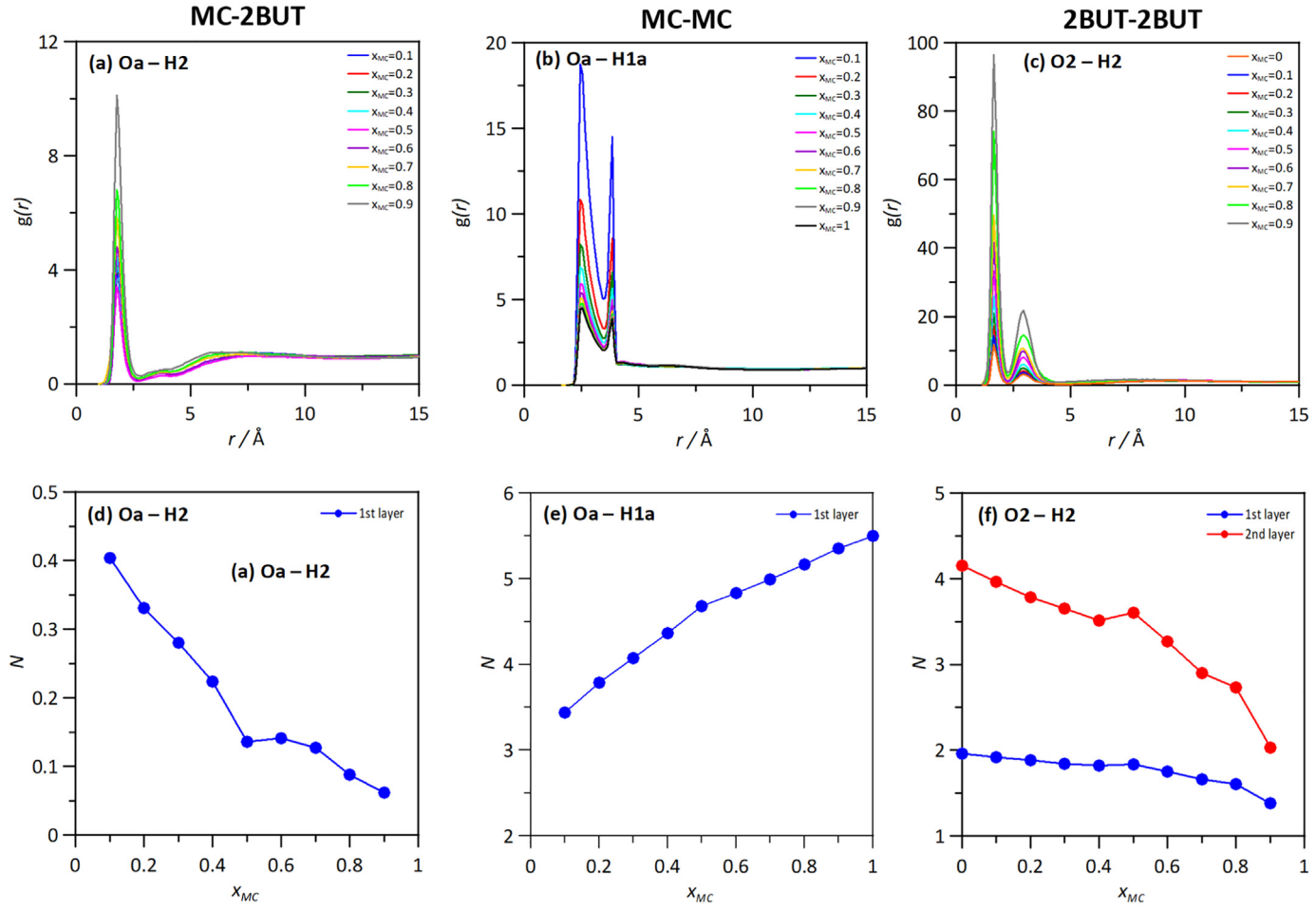

Fig. 8. Site-site radial distribution functions, $g(r)$, and the corresponding solvation numbers, N, for the reported pairs in x MC + (1-x) 2BUT from MD simulations at 313 K and 1 bar. Atom labelling as in Fig. 1. N values were obtained from the integration of $g(r)$ up to the first or second minima, 1st and 2nd layer, respectively.

hydrogen bonding as well as van der Waals interactions is confirmed by the RDG scatter plots reported in Fig. S3 (Supplementary Information). Likewise, the possible charge transfer between the involved molecules was analysed and for that purpose total ChelpG charges were calculated for the optimized dimers showing almost negligible effect for all the considered pairs, thus discarding this mechanism for the stabilization of pairs. HOMO and LUMO orbitals were calculated as well as the corresponding gap and reported in Table 1. The HOMO-LUMO gap is in the 6.3 to 6.6 eV range for the considered systems, with slightly lower values for dimers containing EM than MC and almost negligible alcohol effect. The HOMO orbital is located in the corresponding alcohol whereas the LUMO is in the FAE for all the cases, with shapes independent of the type of FAE but HOMO slightly changing with the type of alcohol. The properties of the reported frontier orbital confirm the hydrogen bonding with the alcohol acting as donor and the FAE as acceptor. The interacting orbitals are located in the region comprising the FAE carbonyl group and the alcohol hydroxyl(s) site.

DFT results confirmed and quantified FAE – alcohol hydrogen bonding but the use of dimers for the calculations does not allow to infer other relevant features (such as larger clustering, molecular packing, steric or long-range effects) which may be present in the liquid blends, which are studied using MD simulations. FAE – alcohol blends are studied using MD in the whole composition range. The structural properties of the considered mixtures are firstly analysed by using selected radial distribution functions, RDFs. It should be remarked that FAEs may act as hydrogen bond acceptors only whereas alcohols can be both donors and acceptors. Therefore, the most relevant RDFs for the analysis of intermolecular interactions are reported in Fig. 8 for MC – 2BUT mixtures in the whole composition range. In this case, MC – 2BUT heteroassociations by hydrogen bonding can be developed through the hydroxyl site (H2 atom) of the alcohol and the CO (Oa) site in the ester, Fig. 1. The reported results for Oa – H2 RDFs in Fig. 8a show a first strong and narrow peak with maxima at 1.8 Å, which confirm that MC and 2BUT are hydrogen bonded. The FAEs – alcohol hydrogen bonding has been reported in previous work for other (longer chains and insaturated) types of FAEs (palmitic, oleic, linoleic) and shorter alcohols (ethanol) [33], and thus the trend reported in this work confirms these results for the light fraction of biodiesels. Likewise, the position of this peak is maintained in the whole composition range, thus confirming heteorassociation through hydrogen bonding in the whole composition range. The integration of RDFs leads to the corresponding solvation numbers, N, i.e. number of atoms around a central one. The N values for Oa – H2 interactions, Fig. 8d, confirm a non-linear behaviour with mixture composition, thus showing two regions up to equimolar mixtures and from that to neat MC, which will lead to mixtures non-ideal behaviour in a thermodynamic sense. For the case of homoassociations, MC-MC (Fig. 8b) and 2BUT – 2BUT (Fig. 8c), large self-interactions are inferred. RDFs for MC – MC interactions, Fig. 8b, show well defined and narrow peaks, although the first peak at 2.6 Å discards hydrogen bonding but MC molecules tend to be self-associated through the COO groups by strong dipolar interactions in the whole composition range. The N values in Fig. 8e show a non-linear evolution with composition with values larger than a pure mixture composition effect, thus confirming strong trend of MC molecules

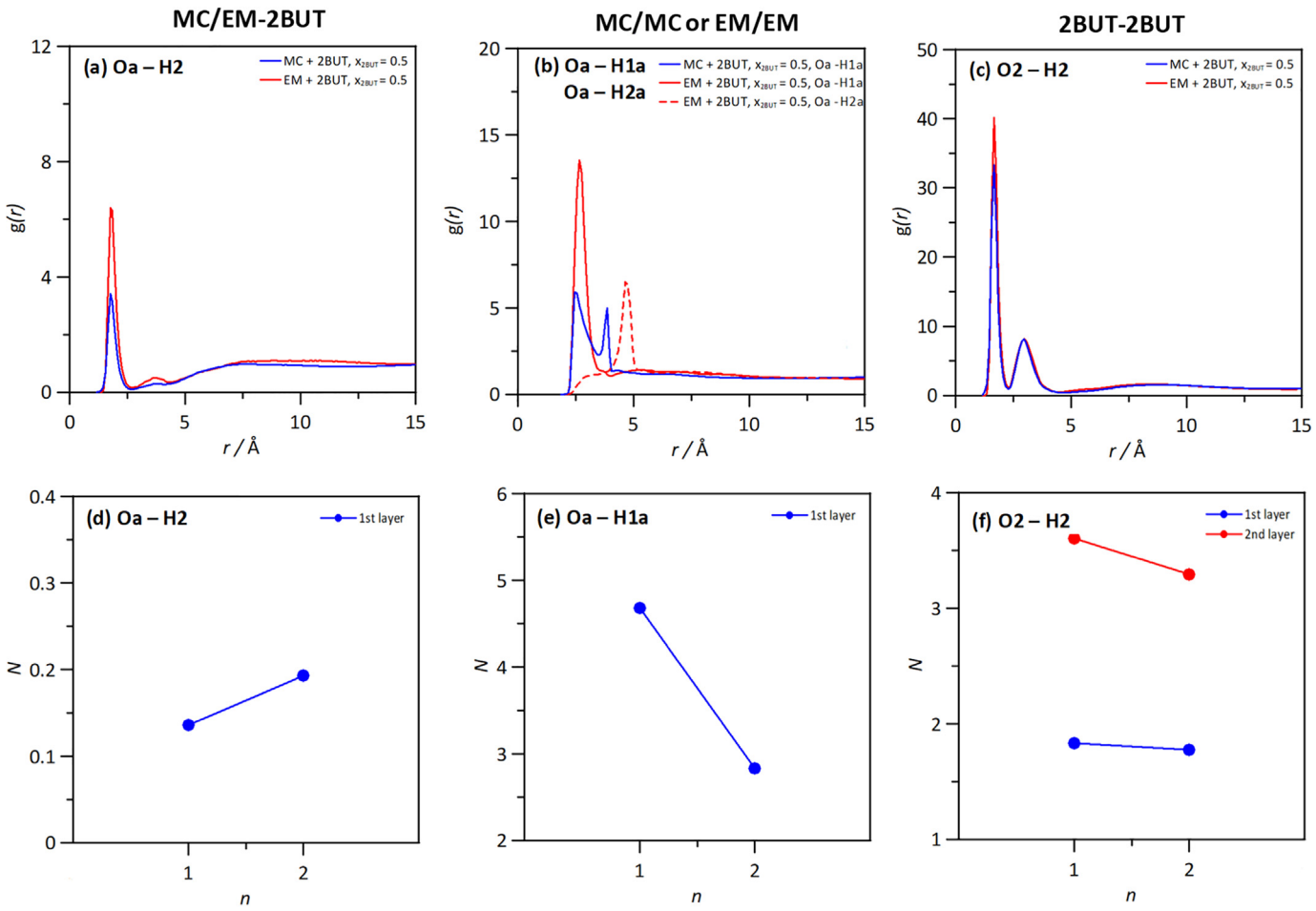

Fig. 9. Site-site radial distribution functions, $g(r)$, and the corresponding solvation numbers, N, for the reported pairs in x {MC or EM} + (1-x) 2BUT (for $x = 0.5$) from MD simulations at 313 K and 1 bar. Atom labelling as in Fig. 1. N values were obtained from the integration of $g(r)$ up to the first or second minima, 1st and 2nd layer, respectively. In panels d to f, $n = 1$ and $n = 2$ stand for MC and EM, respectively.

to be self-aggregated. In the case of 2BUT, RDFs in Fig. 8c show a first narrow and strong peak at 1.7 Å, showing self-hydrogen bonding in the whole composition range, with the corresponding N values larger than linear composition evolution. Therefore, although hetero-associations are inferred in the whole composition range, the trend of both MC and 2BUT to be self-associated is maintained in the whole composition range as in may be inferred from N values in Figs. 8d to 8f.

The effect of the type of FAE on the intermolecular interactions, RDFs, is analysed in Fig. 9 for equimolar mixtures. In the case of FAE – 2BUT interactions (heteroassociations), RDFs in Fig. 9a indicate negligible effect on the mechanism of heteroassociation on going from MC to EM, as the shape of RDFs and position of the maxima are the same for both FAEs. Nevertheless, RDFs first peak is more intense for EM than for MC, Fig. 9a, which lead to larger number of alcohol solvating molecules, but maintaining the mechanism of -interactions, Fig. 9a, i.e. FAE – alcohol hydrogen bonding for both FAEs. This effect can be justified considering the larger size of EM, which allows to fit a larger number of molecules around the hydrogen bonding acceptor sites in the FAE.

For homoassociations, EM presents slightly different self-interaction mechanism, Fig. 9b, although the prevailing interaction between the CO group and the -CH2- group is maintained in spite to the presence of an additional terminal methyl group. For 2BUT – 2BUT hydrogen bonding, it is reinforced on going from MC to EM. The alcohol effect on RDFs is analyzed in Fig. 10, thus showing that the most relevant features are independent on the considered alcohol. MC – alcohol heteroassociation, Fig. 10a, show RDFs almost with identical shape for the studied alcohols, the first RDF peak appears at the same distance and only distributions beyond this first direct short contact change with the type of alcohol. Results for N in Fig. 10d indicate a slight increase in the number of interactions on going to 12BD, per site. In the case of MC – MC self - associations, Fig. 10b, the type of alcohol does not change the mechanism of FAEs self-interaction, only a slight decrease in the number of MC self-associated molecules is inferred on going to 12BD, Fig. 10e, which may be justified considering larger number of heteroassociations, Fig. 10d, thus larger competition between homo and heteroassociations for 12BD than for the other alcohols. Alcohol self-hydrogen bonding, Fig. 10c, show differences between the considered alcohols. In the case of 2BUT and 2M1BUT, the presence of a single hydroxyl group leads to analogous hydrogen bonding, with almost negligible effect because of the presence of an additional methyl group in 2M1BUT, as it is for heteroassociations with MC, Fig. 10a. In the case of 12BD, the presence of two hydroxyl groups leads to a competing effect, as for heteroassociations (Fig. 10a), with a decrease in the number of interactions per site, Fig. 10f, but the hydrogen bonding is maintained as for the other alcohols.

The distribution around each type of molecule in the studied mixtures is analyzed through Spatial Distribution Functions (SDFs) reported in Fig. 11 for FAE + alcohol equimolar mixtures. For central FAE molecules, results confirm that both other FAE molecules as well as the corresponding alcohols concentrate around the COO site of the FAE, although both molecules do not occupy exactly the same regions around the COO group because alcohol molecules are placed closer to the CO groups for developing heteroassociations through hydrogen bonding. Likewise, the type of FAE as well as of alcohol lead to changes

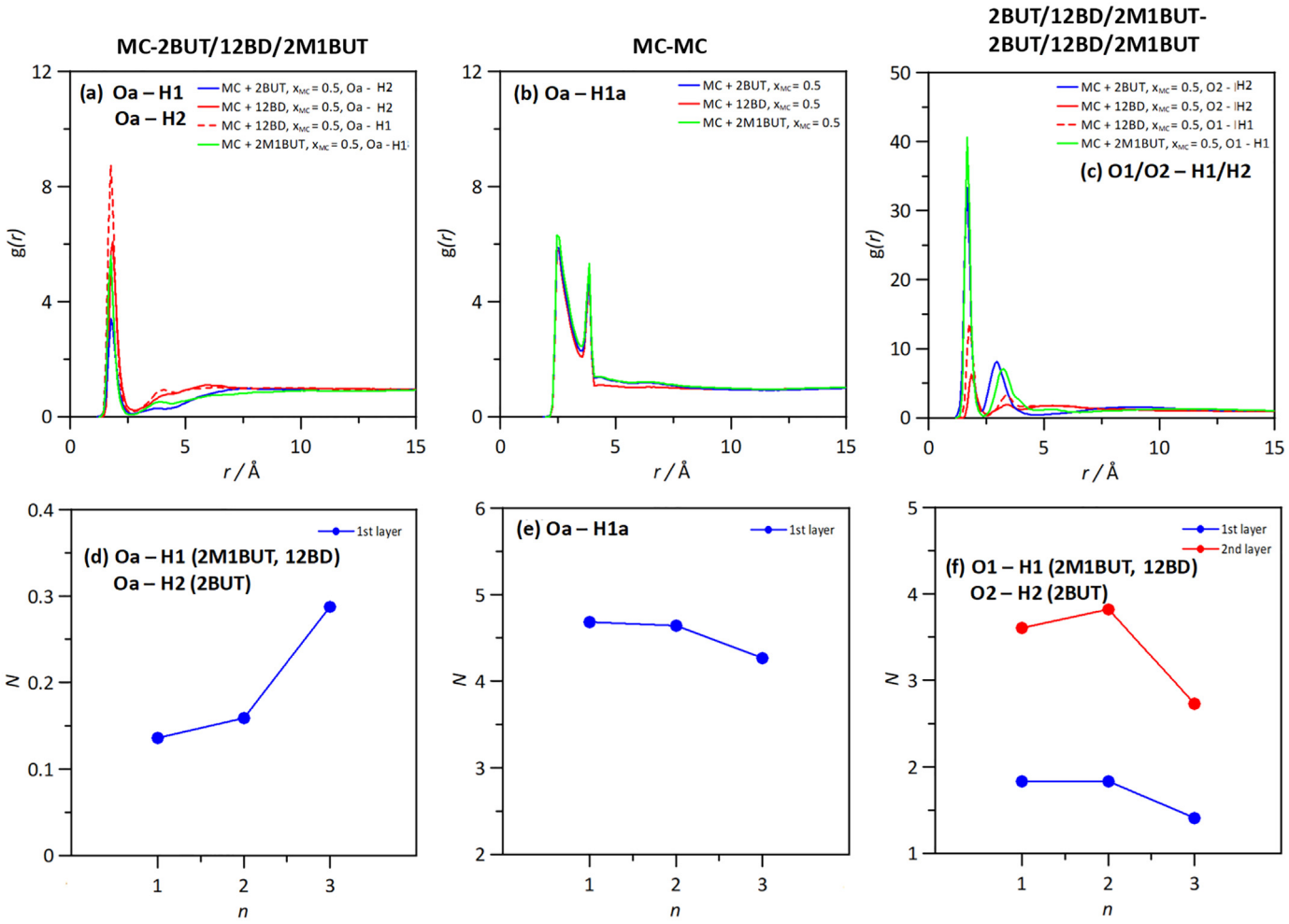

Fig. 10. Site-site radial distribution functions, $g(r)$, and the corresponding solvation numbers, N,for the reported pairs in x MC + (1-x) {2BUT or 2M1BUT or 12BD} (for $x = 0.5$) from MD simulations at 313 K and 1 bar. Atom labelling as in Fig. 1. N values were obtained from the integration of $g(r)$ up to the first or second minima, 1st and 2nd layer, respectively. In panels d to f, $n = 1$, $n = 2$ and $n = 3$ stand for 2BUT, 2M1BUT and 12BD, respectively.

in the SDFs around a central FAE molecule, thus although RDFs in Figs. 9 and 10 showed very minor changes depending on the FAE or the alcohol, the different sizes and position of the hydrogen bonding groups leads to particular arrangements around the FAE COO groups to fit neighbor molecules allowing efficient homo and heteroassociations. In the case of central alcohol molecules, the concentration of alcohol and FA molecules around the hydroxyl sites is confirmed for all the studied systems. Therefore, localized homo and heteroassociations are confirmed in all the cases around the COO (FAE) and OH (alcohol) groups, which will determine all the properties of the considered liquid mixtures in the whole composition range.

The strength of intermolecular interactions is quantified though the intermolecular interaction energy, E_{inter}, which consider electrostatic and van der Waals interactions, Fig. 12. The trend of FAE – alcohol molecules to develop hydrogen bonding as showed by RDFs is confirmed through E_{inter}, with large values being reported in the whole

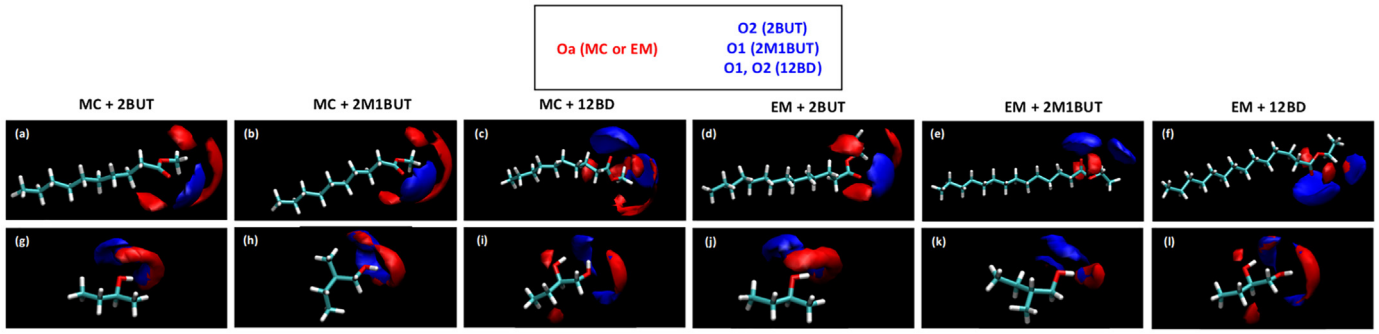

Fig. 11. Spatial distribution functions around (a to f) {MC or EM} or around (g to l) alcohol in x {MC or EM} + (1-x) {2BUT or 2M1BUT or 12BD} ($x = 0.5$) from MD simulations at 313 K and 1 bar. Atom labelling as in Fig. 1.

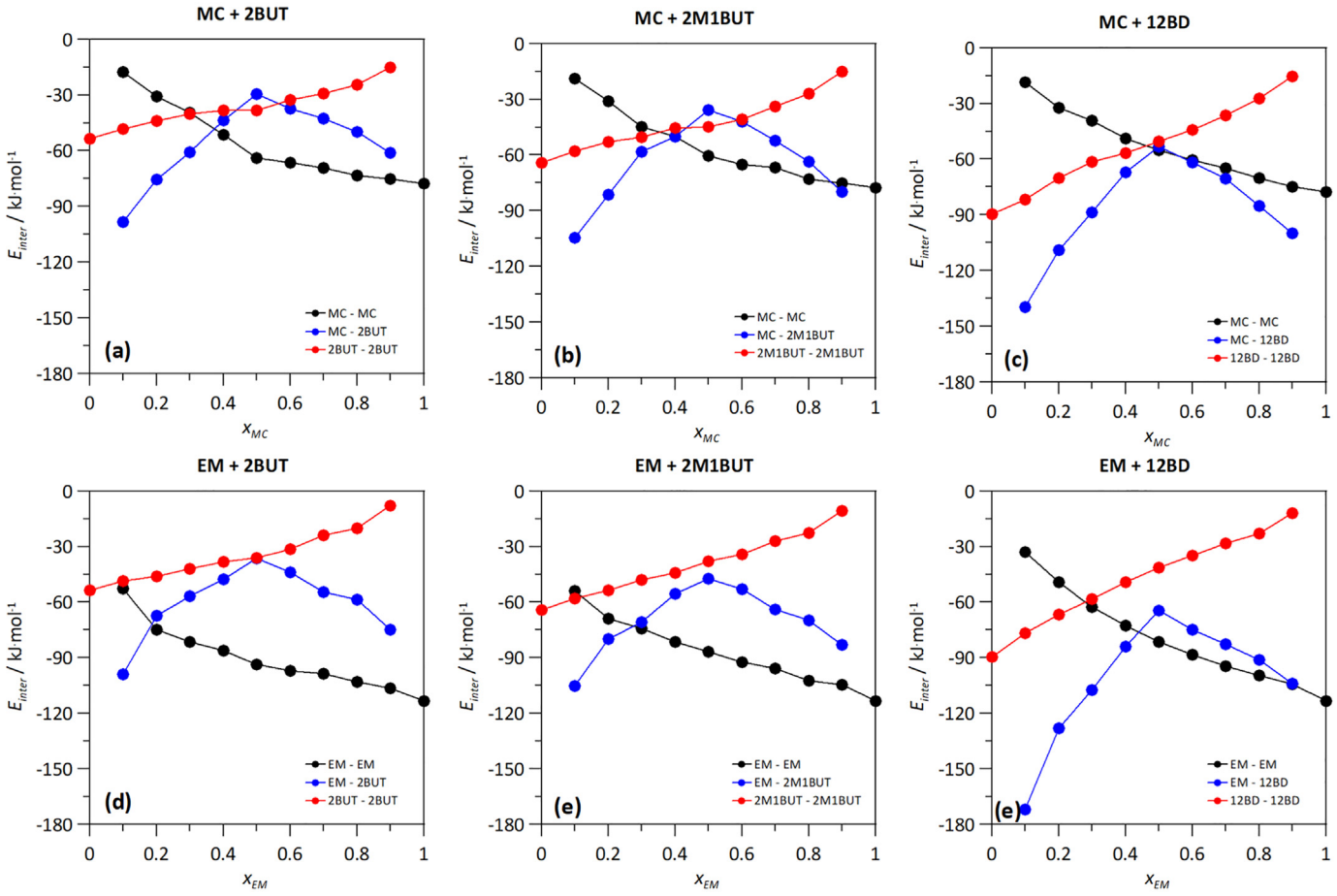

Fig. 12. Intermolecular interaction energy, E_{inter}, for the reported molecular pairs in x {MC or EM} + (1-x) {2BUT, 2M1BUT or 12BD} from MD simulations at 313 K and 1 bar.

composition range for all the alcohols and MC or EM. Likewise, FAE – FAE and alcohol – alcohol interactions are characterized by large E_{inter} also in the whole composition range. These E_{inter} values for all the possible pairs confirm that FAE – alcohol liquid mixtures are characterized by a competing effect of homoassociations with heteroassociations through hydrogen bonding. The absence of FAE – FAE hydrogen bonding does not discard large self-association through dipolar interactions as well as the presence of COO acceptor groups allows a large hydrogen bonding with alcohols, with prevailing interaction depending on the concentration range but with all of them present in the full composition range. This behavior is confirmed the composition evolution of the number of hydrogen bonds per molecule, N_H, as reported in Fig. 13. The N_H values were calculated with a geometrical criterion considering 3.5 Å and 60° for donor – acceptor separation and angle, respectively. The reported N_H values show non-linear evolution with composition, which agrees with a non-ideal mixture behavior in a thermodynamics sense, both for FAE – alcohol as well as for alcohol – alcohol interactions. The N_H values for FAE – alcohol (MC – 2BUT) is lower than the linear evolution, i.e. although hydrogen bonding is developed the number of hydrogen bonds per MC molecule is lower than the pure composition effect. This behavior is produced by the N_H for alcohol – alcohol (2BUT – 2BUT), which are larger than composition linear evolution. Therefore, a reinforcement of alcohol – alcohol hydrogen bonds is produced at cost of the FAE – alcohol interactions, although these heteroassociations are present in the whole composition range.

The evolution and strength of intermolecular forces in the mixtures determine the dynamic behavior of the involved molecules. Mean square displacement, *msd*, was calculated for all the considered mixtures and from there self-diffusion coefficients, D, were determined using Einstein's equation. Results for MC – 2BUT mixtures are reported in Fig. 14. The evolution of *msd* both for MC and 2BUT show that fully diffusive behavior has been reached for all the considered compositions, Figs. 14a and 14b, thus assuring the reliability of calculated D values. The

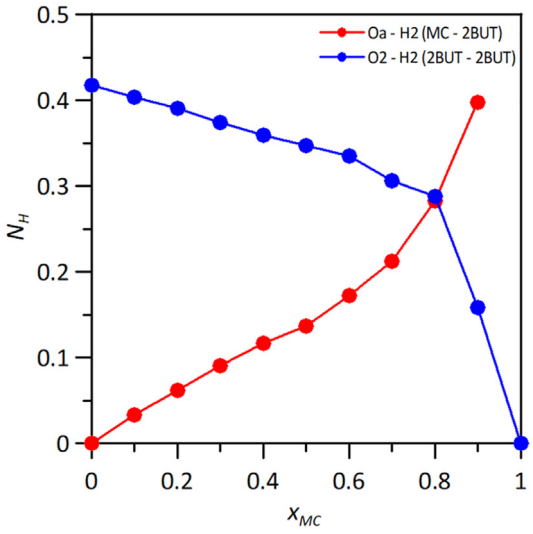

Fig. 13. Average number of hydrogen bonds per 2BUT molecule for the reported pairs in x MC + (1-x) 2BUT from MD simulations at 313 K and 1 bar. Hydrogen bonding criteria: 3.5 Å and 60° for donor – acceptor separation and angle.

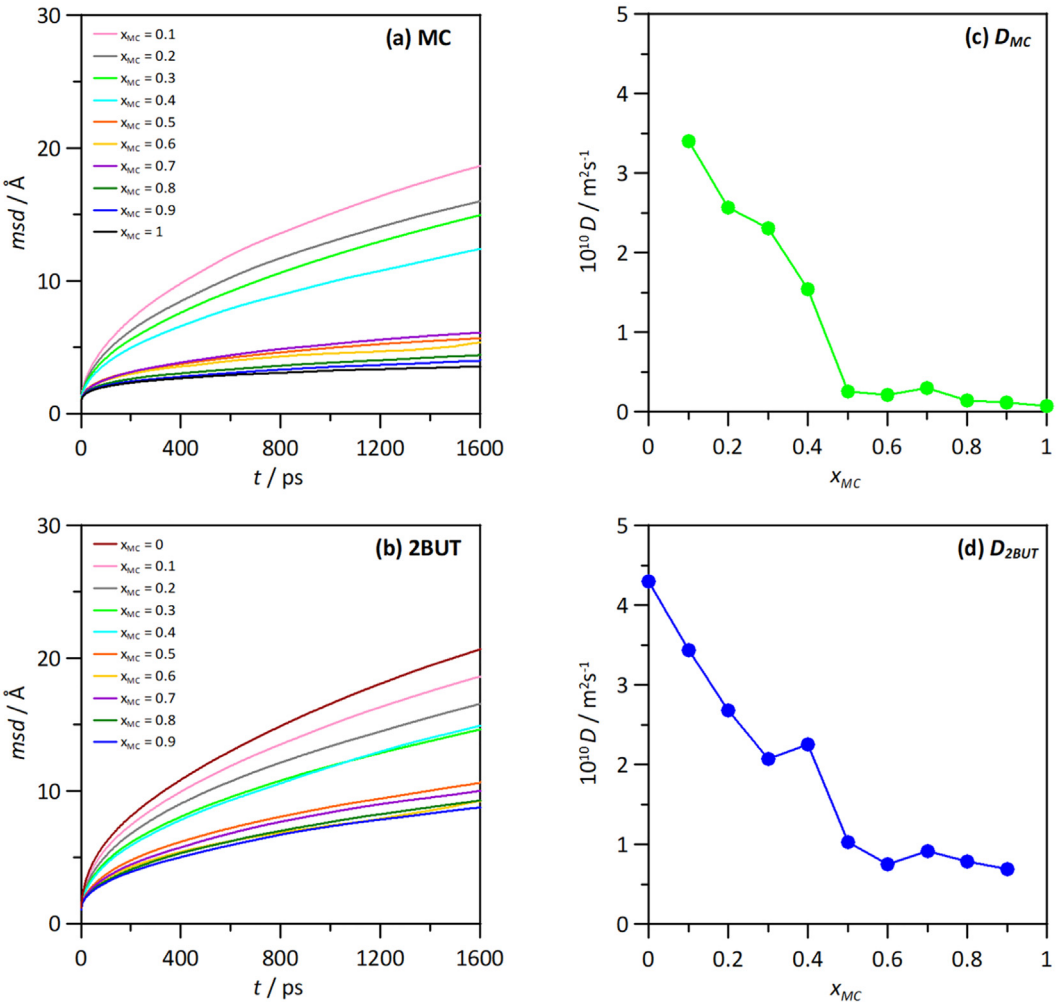

Fig. 14. (a,b) Mean square displacements, *msd*, and (c,d) the corresponding self-diffusion coefficients, *D*, for (a,c) MC and (b.d) 2BUT in *x* MC + (1-*x*) 2BUT from MD simulations at 313 K and 1 bar. *D* values obtained from *msd* using Einstein's equation.

D values for MC, Fig. 14c, and 2BUT, Fig. 14d, show a non-linear evolution with mixture composition, steeply decreasing up to roughly equimolar compositions and then remaining almost constant. This behavior corresponds to the disrupting effect of MC on the alcohol self-hydrogen bonding network because of the competing effect of MC for hydrogen bonding donor sites in the alcohol. The compositions beyond equimolar mixtures are MC (FAE) dominated, thus corresponding to viscous fluids with slow dynamics characterized by MC – MC self – association as well as MC – MC dipolar interactions with minor extension of alcohols self-association. On the contrary alcohol rich mixtures are characterized by a large perturbative effect with increasing MC content, leading to a large decrease of molecular mobility. The reported dynamic properties confirm the role of hydrogen bonding in the studied mixtures with the competing effect because of the presence of FAEs acceptor site for the alcohol hydroxyl groups.

4. Conclusion

This paper has employed a combined experimental and theoretical approach to study the macro and microscopic properties of fatty acids ester mixtures with alcohols with attention to the developed intermolecular forces, mainly hydrogen bonding, as well as their effect on macroscopic blends behavior. All the studied systems showed the non-ideal behavior with ideality deviation pointing to breaking alcohol self-hydrogen bonding as the main effect on the mixtures structure, which is not totally balanced or overcome by the developed ester to alcohol heteroassociations by hydrogen bonding. Quantum chemistry study confirmed that ester – alcohol interactions are moderately weak hydrogen bonding. Molecular dynamics simulations quantified the composition effect on heteroassociations, showing the ability of fatty acid ester top develop hydrogen bonding with alcohols hydroxyl site, weakening alcohol-alcohol interactions, specially for compositions beyond equimolar mixtures. The reported results show that fatty acid ester + alcohol mixtures are characterized by homo and heteroassociations through hydrogen bonding, which are present in the whole composition range and determine molecular mobility, nanostructuring as well as macroscopic thermophysical properties. This study provides for the first time a characterization of modified biodiesels by the addition of alcohols considering light fractions and oils poor in unsaturated fatty acid esters, which can contribute to the understanding of these poorly known oils for the bioenergy industry.

Supplementary data to this article can be found online at https://doi.org/10.1016/j.molliq.2021.115864.

Author statement

The individual contributions to the paper were as follows:

- Dr. H. Ghazipour. Shiraz University of Technology University. Iran. CONTRIBUTION: investigation, formal analysis, data curation, visualization.

- Dr. A. Gutiérrez. University of Burgos. Spain. CONTRIBUTION: investigation, formal analysis, data curation, visualization.
- Prof. S.M. Hosseini. University of Hormozgan. Iran. CONTRIBUTION: conceptualization, formal analysis, writing-original draft, writing-review&editing.
- Prof. S. Aparicio. University of Burgos. Spain. CONTRIBUTION: conceptualization, investigation, methodology, resources, writing-original draft, writing-review&editing, supervision, project administration, funding acquisition.
- Prof. D. Mohammad-Aghaie. Shiraz University of Technology University. Iran. CONTRIBUTION: conceptualization, investigation, methodology, resources, writing-original draft, supervision, project administration.
- Prof. M. M. Alavianmehr. Shiraz University of Technology University. Iran. CONTRIBUTION: conceptualization, investigation, methodology, resources, writing-original draft, supervision, project administration.

Declaration of Competing Interest

The authors whose names are listed immediately below certify that they have NO affiliations with or involvement in any organization or entity with any financial interest (such as honoraria; educational grants; participation in speakers' bureaus; membership, employment, consultancies, stock ownership, or other equity interest; and expert testimony or patent-licensing arrangements), or non-financial interest (such as personal or professional relationships, affiliations, knowledge or beliefs) in the subject matter or materials discussed in this manuscript.

Acknowledgement

The authors wish to thank Shiraz University of Technology (Iran), Junta de Castilla y León (Spain, project BU094G18) and Ministerio de Ciencia, Innovación y Universidades (Spain, project RTI2018-101987-B-I00) for supporting this project. We also acknowledge SCAYLE (Supercomputación Castilla y León, Spain) for providing supercomputing facilities. The statements made herein are solely the responsibility of the authors.

References

[1] G. Knothe, L.F. Razon, Biodiesel fuels, Prog. Energy Combust. Sci. 58 (2017) 36–59.
[2] C.R. Coronado, J.A. de Carvalho, J.L. Silveira, Biodiesel CO_2 emissions: A comparison with the main fuels in the Brazilian market, Fuel Process. Technol. 90 (2009) 204–211.
[3] V.K. Shahir, C.P. Jawahar, P.R. Suresh, Comparative study of diesel and biodiesel on CI engine with emphasis to emissions—a review, Renew. Sust. Energ. Rev. 45 (2015) 686–697.
[4] D. Huang, H. Zhou, L. Lin, Biodiesel: an alternative to conventional fuel, Energy Procedia 16 (2012) 1874–1885.
[5] S.N. Gebremariam, J.M. Marchetti, Economics of biodiesel production: review, Energy Convers. Manag. 168 (2018) 74–84.
[6] B. Sajjadi, A.A.A. Raman, H. Arandiyan, A comprehensive review on properties of edible and non-edible vegetable oil-based biodiesel: composition, specifications and prediction models, Renew. Sust. Energ. Rev. 63 (2016) 62–92.
[7] A.E. Atabani, A.S. Silitonga, I.A. Badruddin, T.M.I. Mahlia, H.H. Masjuki, S. Mekhilef, A comprehensive review on biodiesel as an alternative energy resource and its characteristics, Renew. Sust. Energ. Rev. 16 (2012) 2070–2093.
[8] S.K. Hoekman, A. Broch, C. Robbins, E. Ceniceros, M. Natarajan, Review of biodiesel composition, properties, and specifications, Renew. Sust. Energ. Rev. 16 (2012) 143–169.
[9] L.C. Meher, D.V. Sagar, S.N. Naik, Technical aspects of biodiesel production by transesterification—a review, Renew. Sust. Energ. Rev. 10 (2006) 248–268.
[10] P. Verma, M.P. Sharma, Review of process parameters for biodiesel production from different feedstocks, Renew. Sust. Energ. Rev. 62 (2016) 1063–1071.
[11] T.K. Jose, K. Anand, Effects of biodiesel composition on its long term storage stability, Fuel 177 (2016) 190–196.
[12] W.N.M.W. Ghazali, R. Mamat, H.H. Masjuki, G. Najafi, Effects of biodiesel from different feedstocks on engine performance and emissions: a review, Renew. Sust. Energ. Rev. 51 (2015) 585–602.
[13] H.M. Mahmudul, F.Y. Hagos, R. Mamat, A.A. Adam, W.F.W. Ishak, R. Alenezi, Production, characterization and performance of biodiesel as an alternative fuel in diesel engines – a review, Renew. Sust. Energ. Rev. 72 (2017) 497–509.
[14] E. Buyukkaya, Effects of biodiesel on a DI diesel engine performance, emission and combustion characteristics, Fuel 89 (2010) 3099–3105.
[15] M. Mohamed, C.K. Tan, A. Fouda, M.S. Gad, O. Abu-Elyazeed, A.G. Hashem, Diesel engine performance, emissions and combustion characteristics of biodiesel and its blends derived from catalytic pyrolysis of waste cooking oil, Energies 13 (2020) 5708.
[16] J.J. Cano-Gómez, G.A. Iglesias-Silva, P. Rivas, C.O. Díaz-Valle, F.J. Cerino-Córdova, Densities and viscosities for binary liquid mixtures of biodiesel + 1-butanol, + isobutyl alcohol, or + 2-butanol from 293.15 to 333.15 K at 0.1 MPa, J. Chem. Eng. Data 62 (2017) 3391–3400.
[17] A. Török, Theoretical estimation of the environmental impact of biofuel mixtures, Transport 24 (2009) 26–29.
[18] R. Niculescu, A. Clenci, V. Iorga-Siman, Review on the use of diesel–biodiesel–alcohol blends in compression ignition engines, Energies 12 (2019) 1194.
[19] H. Aydin, C. Ilkilic, Effect of ethanol blending with biodiesel on engine performance and exhaust emissions in a CI engine, Appl. Thermal Energy 30 (2010) 1199–1204.
[20] N. Yilmaz, F.M. Vigil, K. Benalil, S.M. Davis, A. Calva, Effect of biodiesel-butanol fuel blends on emissions and performance, Fuel 135 (2014) 46–50.
[21] G. Knothe, Improving biodiesel fuel properties by modifying fatty ester composition, Energy Environ. Sci. 2 (2009) 759–766.
[22] G. Knothe, "Designer" Biodiesel: optimizing fatty ester composition to improve fuel properties, Energy Fuel 22 (2008) 1358–1364.
[23] A.J. Folayan, P.A.L. Anawe, A.E. Aladejare, A.O. Ayeni, Experimental investigation of the effect of fatty acids configuration, chain length, branching and degree of unsaturation on biodiesel fuel properties obtained from lauric oils, high-oleic and high-linoleic vegetable oil biomass, Energy Rep. 5 (2019) 979–986.
[24] R. Rasyid, Z. Sabara, A. Pratiwi, R. Juradin, R. Malik, The Production of biodiesel from a traditional coconut oil using NaOH/γ-Al_2O_3 heterogeneous catalyst, IOP Conf. Series: Earth Environ. Sci. 175 (2018) 012025.
[25] Z. Zhang, E. Jiaqiang, Y. Deng, M.H. Pham, W. Zuo, Q. Peng, Z. Yin, Effects of fatty acid methyl esters proportion on combustion and emission characteristics of a biodiesel fueled marine diesel engine, Energy Convers. Manag. 159 (2018) 244–253.
[26] M.J. Ramos, C.M. Fernández, A. Casas, L. Rodríguez, A. Pérez, Influence of fatty acid composition of raw materials on biodiesel properties, Bioresour. Technol. 100 (2009) 261–268.
[27] P. Saxena, S. Jawale, M.H. Joshipura, A Review on prediction of properties of biodiesel and blends of biodiesel, Proc. Eng. 51 (2013) 395–402.
[28] A. Datta, B.K. Mandal, Engine performance, combustion and emission characteristics of a compression ignition engine operating on different biodiesel-alcohol blends, Energy 125 (2017) 470–483.
[29] M. Dahmen, W. Marquardt, Model-based formulation of biofuel blends by simultaneous product and pathway design, Energy Fuel 31 (2017) 4096–4121.
[30] I. Pires de Oliveira, A.R.L. Caires, Molecular arrangement in diesel/biodiesel blends: a molecular dynamics simulation analysis, Renew. Energy 140 (2019) 203–211.
[31] V.S. Bharadwaj, N.M. Eagan, N.M. Wang, M.W. Liberatore, C.M. Maupin, molecular simulations of fatty-acid methyl esters and representative biodiesel mixtures, ChemPhysChem 18 (2015) 2810–2817.
[32] H. Luo, W.Y. Fang, Y. Li, G.Z. Nan, Lubrication properties of biodiesel: experimental investigation and molecular dynamics simulations, Appl. Mech. Mater. 316-317 (2013) 1075–1079.
[33] I. Pires de Oilveira, A. Rodrigues Lima Cires, K. Baskar, S. Ponnusamy, P. Laksmanan, V. Veerappan, Biodiesel as an additive for diesel-ethanol (diesohol) blend: physical-chemical parameters and origin of the fuels' miscibility, Fuel 263 (2020) 116753.
[34] A.A. Refaat, Correlation between the chemical structure of biodiesel and its physical properties, Int. J. Environ. Sci. Technol. 6 (2009) 677–694.
[35] N. Nabipour, R. Daneshfar, O. Rezvanjou, M.M. Khnaposhtani, A. Baghban, Q. Xiong, L.K.B. Li, S. Habibzadeh, M.H. Doranehgard, Estimating biofuel density via a soft computing approach based on intermolecular interactions, Renew. Energy 152 (2020) 1086–1098.
[36] F. Neese, The ORCA program system, WIREs Comput. Mol. Sci. 2 (2012) 73–78.
[37] C. Lee, W. Yang, R.G. Parr, Development of the Colle-Salvetti correlation-energy formula into a functional of the electron density, Phys. Rev. B 37 (1988) 785–789.
[38] A.D. Becke, Density-functional exchange-energy approximation with correct asymptotic behavior, Phys. Rev. A 38 (1988) 3098–3100.
[39] A.D. Becke, Density-functional thermochemistry. III. The role of exact exchange, J. Chem. Phys. 98 (1993) 5648–5652.
[40] S. Grimme, J. Antony, S. Ehrlich, H.A. Krieg, A consistent and accurate ab initio parametrization of density functional dispersion correction (DFT-D) for the 94 elements H-Pu, J. Chem. Phys. 132 (2010) 154104.
[41] R.F.W. Bader, Atoms in Molecules: A Quantum Theory, 1990 (Oxford).
[42] E.R. Johnson, S. Keinan, P. Mori-Sanchez, J. Contreras-García, A.J. Cohen, W. Yang, Revealing non-covalent interactions, J. Am. Chem. Soc. 132 (2010) 6498–6506.
[43] T. Lu, F. Chen, Multiwfn: A multifunctional wavefunction analyzer, J. Comput. Chem. 33 (2012) 580–592.
[44] S. Simon, M. Duran, J. Dannenberg, How does basis set superposition error change the potential surfaces for hydrogen-bonded dimers? J. Chem. Phys. 105 (1996) 11024.
[45] C.M. Breneman, K.B. Wiberg, Determining atom-centered monopoles from molecular electrostatic potentials. The need for high sampling density in formamide conformational analysis, J. Comput. Chem. 11 (1990) 361–373.
[46] A.P. Lyubartsev, A. Laaksonen, M. DynaMix, A scalable portable parallel MD simulation package for arbitrary molecular mixtures, Comput. Phys. Commun. 128 (2000) 565–589.
[47] L. Martínez, R. Rade, E.G. Birgin, J.M. Martínez, PACKMOL: a package for building initial configurations for molecular dynamics simulations, J. Comput. Chem. 30 (2009) 2157–2164.

[48] V. Zoete, M.A. Cuendet, A. Grosdidier, O. Michielin, SwissParam, a fast force field generation tool for small organic molecules, J. Comput. Chem. 32 (2011) 2359–2368.
[49] J.B. Parsa, M.F. Haghro, Excess molar volume and viscosity deviation for binary mixturesof polyethylene glycol dimethyl ether 250 with 1,2-alkanediols(C3–C6) atT= (293.15 to 323.15) K, J. Chem. Thermodyn. 40 (2008) 782–788.
[50] M. Tuckerman, B.J. Berne, G.J. Martyna, Reversible multiple time scale molecular dynamics, J. Chem. Phys. 97 (1992) 1990–2001.
[51] U.L. Essmann, M.L. Perera, T. Berkowitz, H. Darden, H. Lee, L.G. Pedersen, A smooth particle mesh Ewald method, J. Chem. Phys. 103 (1995) 8577–8593.
[52] U. Koch, P.L. Popelier, Characterization of C-H-O hydrogen bonds on the basis of the charge density, J. Phys. Chem. 99 (1995) 9747–9754.